The Astrophysical Journal, 693:1022–1028, 2009 March 1 doi:10.1088/0004-637X/693/1/1022

PERSISTENT AND SELF-SIMILAR LARGE-SCALE DENSITY FLUCTUATIONS IN THE SOLAR CORONA

D. Telloni[1], E. Antonucci[1], R. Bruno[2], and R. D'Amicis[2]
[1] Istituto Nazionale di Astrofisica (INAF), Osservatorio Astronomico di Torino, Strada Osservatorio 20, 10025, Pino Torinese, Italy
[2] Istituto Nazionale di Astrofisica (INAF), Istituto di Fisica dello Spazio Interplanetario, Via del Fosso del Cavaliere, 100, 00133, Roma, Italy
Received 2008 September 22; accepted 2008 November 27; published 2009 March 3

ABSTRACT

Density fluctuations of the low and midlatitude solar corona plasma are analyzed during the recent solar minimum period. Long time series of the intensity of the neutral hydrogen Lyα, 1216 Å, line have been observed with the UltraViolet Coronagraph Spectrometer/*Solar and Heliospheric Observatory* at 1.7 $R_{\odot}$, in low-latitude streamers and in regions where the slow solar wind is accelerated. Their frequency composition is investigated by using three different techniques, namely the Fourier, the Hurst, and the phase coherence analyses. The Fourier analysis reveals the existence of low-frequency $f^{-\alpha}$ power spectra in the range from $\sim 3 \times 10^{-6}$ Hz to $\sim 10^{-4}$ Hz, corresponding to periods from a few hours to a few days. The coronal density fluctuations are dominated by discontinuities separating structures with a minimum characteristic timescale of about 3 hr and a corresponding spatial scale of about 3×10^4 km. The nonlinear analysis technique based on the structure functions shows that for large timescales the coronal density fluctuations are statistically self-affine and give rise to an average Hurst exponent $\langle H \rangle = 0.654 \pm 0.008$. This indicates that the process underlying the variability of the corona and the slow wind at coronal level is a persistent mechanism, generating correlations among the plasma density fluctuations. Finally, the analysis based on the phase coherence index shows a high degree of phase synchronization of the coronal density variations for large timescales, which shows that the solar corona is dominated by phase coherent structures. The results of the analysis suggest a coupling of the variability of the solar corona and the photospheric dynamics induced by the convection at supergranular scale.

Key words: solar wind – Sun: atmospheric motions – Sun: corona – Sun: granulation – Sun: oscillations

Online-only material: color figures

1. INTRODUCTION

Power spectra with a frequency dependence of f^{-2} characterize the magnetic field intensity, outflow speed, and density fluctuations of the interplanetary plasma (e.g., Sari & Ness 1969; Coles & Harmon 1978; Burlaga & Mish 1987; Roberts & Goldstein 1987). Fluctuations exhibiting the same power-law spectra have been recently observed when analyzing the plasma density in polar coronal holes, where the fast solar wind originates (Bemporad et al. 2008). Whilst the $1/f$ flicker noise is interpreted as a consequence of a superposition of signals with different statistical properties (Matthaeus & Goldstein 1986; Matthaeus et al. 2007), the $1/f^2$ Brownian noise is typical of time series dominated by discontinuities, which could be due to a variety of phenomena, such as, for instance, MHD shocks, magnetoacoustic waves propagating outward from the Sun, tangential discontinuities separating convected plasma regions, such as magnetic flux tubes as observed in interplanetary space (Bruno et al. 2001). The above results were obtained by applying a harmonic analysis based on discrete Fourier transforms, which reveals periodicities in the input data as well as the relative strengths of the periodic components.

Other authors, instead, have applied the Hurst analysis to study the variability of solar data. This nonlinear technique, based on the structure functions which are described in Section 3.2., allows us to understand whether the observed fluctuations are caused by a persistent and correlated process. Moreover, the analysis allows us to investigate the scaling properties of the variations found in the time records. For instance, Nesis et al. (1994) investigated the dynamics of solar granulation by studying photospheric intensity fluctuations which were found to be persistent. Komm (1995) observed a high degree of persistency in the temporal variation of the solar rotation on timescale shorter than the 11 year cycle. For what concerns phenomena directly related to solar activity, a high degree of persistency has been observed in the monthly sunspot number variations (Mandelbrot & Wallis 1969), in the tree-ring ^{14}C radiocarbon data (Ruzmaikin et al. 1994), and in the intensity variations of the optical flares analyzed by Lepreti et al. (2000), who find the results in agreement with those by Mandelbrot & Wallis (1969).

In order to quantify the phase synchronization in nonlinear interactions, Hada et al. (2003) have developed a nonlinear technique based on the phase coherence index, which is described in Section 3.3. This allows us to determine whether or not the observed data are characterized by coherent structures. On the basis of this approach, these authors have established the existence of phase coherence of MHD waves in the Earth foreshock region.

The present paper aims to extend to the outer corona the investigation on periodicities and on the presence of persistent and coherent structures in the solar plasma, by analyzing the density fluctuations derived from the H I Lyα 1216 Å intensity variations. The Lyα emission has been observed with UltraViolet Coronagraph Spectrometer (UVCS)/*Solar and Heliospheric Observatory* (*SOHO*) in an interval of about two weeks in 2007 December, during the recent solar minimum. The observations were performed at low and midlatitudes, thus allowing us to study also the possible latitudinal effects. The regions of the outer corona involved in the analysis are coronal streamers and slow wind acceleration regions, which are characterized by different magnetic configurations. Coronal density observations are examined with the three main techniques of investigation used in the literature, namely (1) the

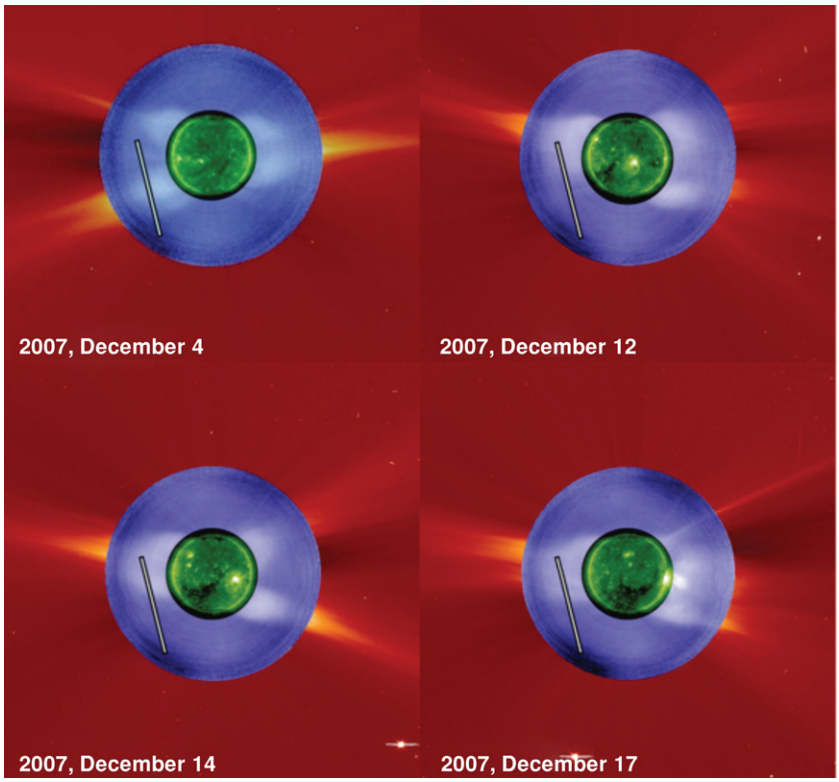

Figure 1. LASCO C2, Mark IV, and EIT 195 Å composite image of the solar corona on 2007 December 4-12-14-17; the white thick line indicates the position and size of the slit.

(A color version of this figure is available in the online journal.)

standard Fourier analysis, (2) the Hurst (Hurst 1951; Mandelbrot & Wallis 1969), and (3) Hada et al. (Hada et al. 2003) nonlinear techniques. The last two diagnostic methods are for the first time applied to observations performed in the outer solar corona.

In order to search for scaling laws in the coronal density variations, we apply the Fourier analysis to the time series of the Lyα line intensity. Successively, the Hurst technique is applied in order to search for evidence for persistency and self-similarity and thus to establish the nature of the coronal density fluctuations and their scale properties on various timescales. At last, the Hada et al. (2003) analysis is performed in the attempt to find coherent structures in the density fluctuations. These studies allow us to investigate a possible coupling of the variability of the solar corona, on temporal scales larger than a few hours, and the photospheric and convection zone dynamics, by comparing the analysis results with those inferred from analogous studies performed on photospheric data.

2. OBSERVATIONS

The analysis is applied to the observations performed with the UVCS (Kohl et al. 1995), onboard the *SOHO*. For about 13.4 days during the solar activity minimum of the 23rd cycle, from 16:42 UT on 2007 December 3 to 07:54 UT on 2007 December 17, the instrument observed continuously the equatorial and midlatitude coronal region delimited by the spectrometer slit, as shown in Figure 1.

The Lyα line, emitted by the neutral hydrogen atoms at 1216 Å, is detected in an instantaneous field of view (FOV) ($30' \times 84''$) wide. The slit, set at 1.7 $R_\odot$ at the east limb, is oriented in such a way to cover a broad latitude range, from 7° northeast (NE) to 51° southeast (SE). The sampling time $\Delta t = 120$ s has been chosen to perform a spectral analysis in a broad frequency range, from 8×10^{-7} Hz up to the Nyquist–Shannon frequency $f_{\rm NS} = 1/(2\Delta t) = 4 \times 10^{-3}$ Hz.

The observed H I Lyα intensity fluctuations are caused uniquely by variations of the physical properties of the emitting coronal plasma crossing the slit FOV, since, as discussed by Morgan et al. (2004), the UVCS instrumental contributions to the temporal variability of the line intensity can be neglected. Photon-shot noise, associated with the random arrival of photons on the detector, does not affect significantly the observations, since the count rate is everywhere larger than the Poisson statistic fluctuations (about 3 Hz).

The emission of the H I Lyα line is mainly due to resonant scattering of the ultraviolet photons emitted from the lower layers of the atmosphere, namely the chromosphere and transition region (Gabriel 1971). The fluctuations of the Lyα line intensity $\langle \delta I\,(\mathrm{Ly}\alpha)^2 \rangle$ are primarily related to those of the hydrogen coronal density $n_{\rm H}$, and the outflow speed of the emitting hydrogen atoms, $v_{\rm out}$, via Doppler dimming effect (e.g., Noci et al. 1987). However, in the midlatitude and equatorial regions, the expansion of the solar corona is slow with a speed below 90 km s^{-1} at 1.8 $R_\odot$ (Abbo et al. 2003; Antonucci et al. 2005) and thus the Doppler dimming effect which depends on its outflow velocity can be substantially neglected. At higher latitudes, Bemporad et al. (2008) have shown that a 25% variation in $v_{\rm out}$ implies a corresponding I (Lyα) variation by less than 10%, while a 25% variation in $n_{\rm H}$ implies a corresponding I (Lyα) variation by 25% (I (Lyα) $\propto n_e$). Hence, to a first approximation, the Lyα intensity fluctuations are representative of those of the coronal plasma density integrated along the line of sight (LOS). Since the hydrogen density decreases very rapidly with the increasing heliocentric distance, the most important contribution to the

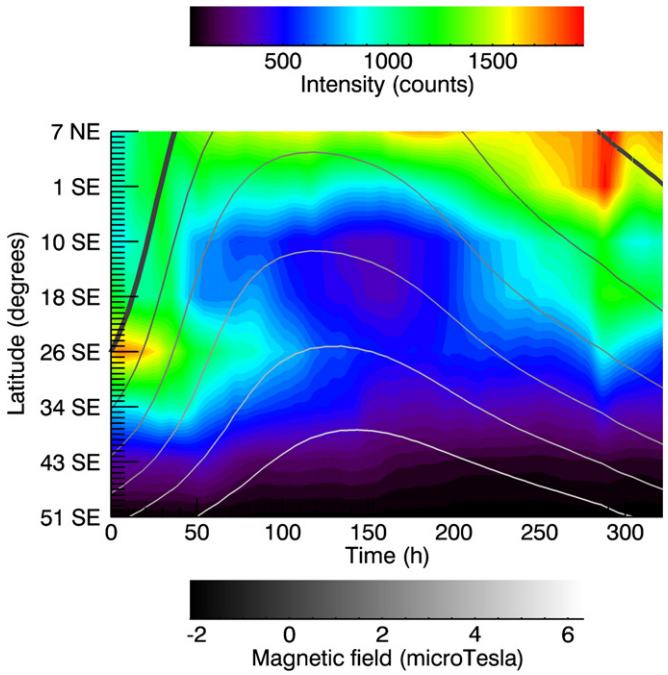

Figure 2. Synoptic map of the H I Lyα line intensity, expressed in count units, as a function of time and heliographic latitude; the thick line, lying on the more intense coronal regions, represents the heliomagnetic equator as provided by the Wilcox Solar Observatory source surface synoptic charts, while the thinner lines show the positive regions of the coronal magnetic field.

(A color version of this figure is available in the online journal.)

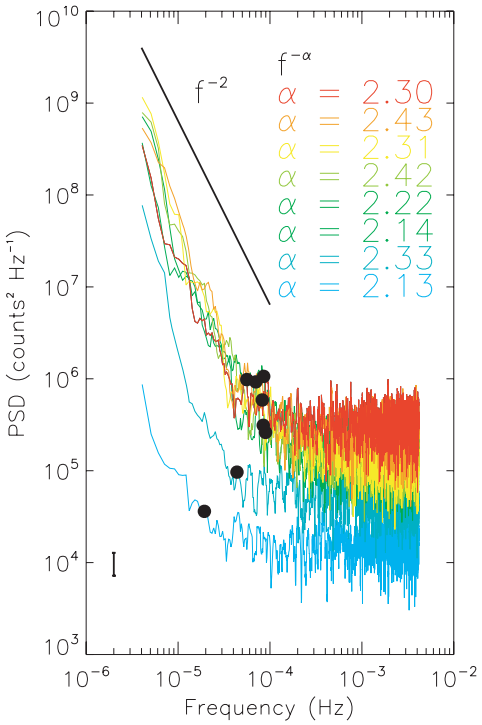

Figure 3. Power spectra of the Lyα intensity time series at heliographic latitudes ranging from 7° NE (red line) to 51° SE (blue line); full black dots represent the knee of the spectrum; the vertical line indicates a confidence level of 95%.

(A color version of this figure is available in the online journal.)

integration is due to the volume element of the corona close to the plane of the sky (POS). It turns out that the fluctuations of H I Lyα emission, observed in corona, can be mainly associated with neutral hydrogen density variations on the POS.

The synoptic map of the intensity of the H I Lyα line, reconstructed on the basis of the UVCS instantaneous FOV images, is shown as a function of time and heliographic latitude in Figure 2.

The neutral line of the coronal magnetic field, calculated from photospheric field observations with a potential field model and provided by the Wilcox Solar Observatory source surface synoptic charts, is shown in Figure 2 as a thick dark line: it lies on the coronal regions where the intensity is larger. The neutral line is a good indicator of the heliomagnetic equator, that is of the central latitude of the equatorial streamers, where the coronal plasma is confined. Therefore, the more intense coronal regions observed with UVCS/*SOHO*, where the count rate exceeds 12.5 counts s^{-1} (the yellow and orange regions of Figure 2), can be considered as coronal streamers.

During solar minimum, the primary sources of the heliospheric slow wind are found in correspondence to the streamer equatorial belt (McComas et al. 2000). In the corona, this region is characterized by large quiescent coronal streamers, which are very likely composed by substreamers, formed by closed loops and separated by open field lines that are channeling a slow plasma that flows close to the heliospheric current sheet (Noci & Gavryuseva 2007). There is evidence, however, for a dominant slow wind component in the corona flowing along the streamer borders at the edges of the polar coronal holes. This result thus indicates that the coronal regions adjacent to the streamer belt are the main sources of the slow solar wind (e.g., Wang & Sheeley 1990; Antonucci et al. 2005, 2006; Wang et al. 2000). Since, for almost the whole time period covered by the observations, the neutral line lies at heliographic latitudes slightly higher than those observed, it turns out that the low and mid-latitude observations are performed most of the time in coronal regions where the slow wind is emerging and accelerated.

The same analyses show a gradual transition from slow to fast wind when moving from the streamer border to the center of the polar coronal holes. Hence, on the basis of the previous solar wind studies during minimum activity, we expect in Figure 2 a gradual variation toward higher velocities of the coronal wind when moving from equatorial regions to higher latitudes.

3. ANALYSIS

The time series of the coronal H I Lyα line intensity obtained at the various latitudes are examined by (1) the Fourier analysis in order to derive the spectral properties and the periodic variations of the time records; (2) the Hurst analysis to determine the scaling, the fractal nature, and the persistent behavior of the coronal density fluctuations; (3) the Hada et al. (2003) analysis to investigate the existence of coherent structures in the solar corona and the degree of phase synchronization in the data records.

3.1. Fourier Analysis

The spectral analysis is performed using a Fast Fourier Transform (FFT) on data samples consisting of $N = 2^n$ elements which, in our case, corresponds to $N = 8192$ measurements. The time series is first linearly detrended and tapered applying a 10% cosine window to eliminate spurious high-frequency power in the spectra. The low-frequency range of the spectrum is fitted with a $(A \cdot f^{-\alpha})$ function, by applying the Levenberg–Marquardt least squares minimization method with a confidence level of 95%, in order to infer the spectral index α.

Figure 3 shows the smoothed power spectra for each heliographic latitude observed: warmer colors indicate equatorial

Table 1
Spectral Index α, Cutoff Frequency f_c, Observed and Expected White Noise as a Function of Heliographic Latitude

Latitude (°)	Spectral Index α	Cutoff Frequency f_c (Hz)	White Noise (counts^2 Hz^{-1})	$\sum_i x_i/(f_{NS} \cdot N)$ (counts^2 Hz^{-1})
7 N	2.30 ± 0.23	5.59×10^{-5}	3.47×10^5	3.78×10^5
1 S	2.43 ± 0.18	7.02×10^{-5}	2.68×10^5	2.67×10^5
10 S	2.31 ± 0.22	8.24×10^{-5}	1.57×10^5	1.64×10^5
18 S	2.42 ± 0.12	8.95×10^{-5}	1.60×10^5	1.68×10^5
26 S	2.22 ± 0.39	8.54×10^{-5}	1.90×10^5	2.05×10^5
34 S	2.14 ± 0.13	8.44×10^{-5}	1.40×10^5	1.39×10^5
43 S	2.33 ± 0.31	4.37×10^{-5}	5.56×10^4	5.70×10^4
51 S	2.13 ± 0.94	1.93×10^{-5}	1.74×10^4	1.73×10^4

regions, while cooler colors indicate regions toward the coronal hole present at the South Pole, following the rainbow scale.

The power of the spectrum decreases with increasing latitude moving from the denser equatorial region toward the more tenuous South coronal hole. Spectra exhibit a power law $f^{-\alpha}$ dependence for at least one decade, in the frequency range from $\sim 4 \times 10^{-6}$ Hz to $\sim 4 \times 10^{-5}$ Hz. That is, the spectral analysis shows the existence of large-scale fluctuations in the coronal plasma density, with periods from a few hours to a few days. The spectral index α is larger than 2, with an average value $\langle \alpha \rangle = 2.36 \pm 0.07$, as reported in the second column of Table 1 as a function of the heliographic latitude.

The power-law spectra flatten out at frequencies higher than 10^{-4} Hz. The frequency f_c, corresponding to the knee which separates these two different spectral regimes, shifts to lower values for observations performed at higher heliographic latitudes. In order to identify the frequency corresponding to the knee, we consider a moving spectral window where the spectrum is fitted with a power-law function. Accordingly, the spectral index varies with frequency from a value close to 2 (see Table 1), in the frequency range where the spectrum exhibits a power-law scaling, to a 0 value where the spectrum is flattening out. The knee is evaluated by inferring at which frequency the spectral index α is equal to the value 1/2. The cutoff frequency ranges from $\sim 9 \times 10^{-5}$ Hz at 18° SE to $\sim 2 \times 10^{-5}$ Hz at 51° SE and it is rather constant in the latitude range 7° NE–34° SE, as reported in the third column of Table 1. In Figure 3, this quantity is plotted as a function of the heliographic latitude (full black dots). The knee shift toward lower frequencies, with increasing heliographic latitude, occurs for latitudes larger than 30°, when approaching the South coronal hole.

The flat spectrum observed at frequencies higher than about 10^{-4} Hz suggests that the short-period fluctuations might be due to white noise caused by statistically independent variations in the observed data. Since UVCS is a spectrometer equipped with a photon-counting detector, the time series are affected by Poisson-distributed noise. The white component, given by the average high-frequency power, is expected to be consistent with the expression σ^2/f_{NS}, where σ^2 is the second moment of the random noise component and f_{NS} is the Nyquist–Shannon frequency. In the Poisson distributions the variance σ^2 is numerically equal to the mean $\sum_i x_i/N$, where $\{x\}$ is the data sample consisting of N elements (Hoyng 1976). Hence, the average power in the white high-frequency part of the spectrum derived from the data can be compared with the expected value $\sum_i x_i/(f_{NS} \cdot N)$ (fourth and fifth columns of Table 1, respectively). The fact that the two values are in fairly good agreement suggests that the high-frequency range is indeed dominated by uncorrelated noise fluctuations.

Power spectra following the f^{-2} scaling do result from discontinuities in the data time series (e.g., Siscoe et al. 1968; Burlaga & Mish 1987; Berton 2004). Thus, since the spectral index found in the analysis is close to 2, the presence of discontinuities in the hydrogen Lyα line intensity, and in turn in the coronal density, can be suggested. These discontinuities can arise either from inhomogeneities carried by the expanding coronal plasma, such as MHD shocks, or magnetoacoustic waves propagating outward. On the other hand, they could be nonpropagating long-lived discontinuities crossing the slit during the solar rotation, and separating spatial structures with different density characteristics, as for instance magnetic flux tubes. It is to be noted that the power spectrum of a superposition of a large number of discontinuities varies as f^{-2}, at frequencies larger than the frequency corresponding to the average separation between the discontinuities (Siscoe et al. 1968). This allows us to estimate the characteristic timescale of the structures separated by two consecutive discontinuities, by inferring their largest frequency, corresponding to the cutoff f_c in the spectra of Figure 3. Hence the lowest period of occurrence of the discontinuities consistent with the observations is defined as $t_{min} = f_c^{-1}$: in the latitude range 7° NE–34° SE it is $t_{min} = f_c^{-1} \sim 10^4$ s $\approx$ 3 hr and becomes larger approaching coronal holes, since the cutoff frequency is smaller at higher heliographic latitudes. If we suppose that these discontinuities mark the border between adjacent radial structures corotating with the Sun, the characteristic dimension of these spatial structures corresponding to $f_c^{-1} \sim 10^4$ s is about 3×10^4 km, value which corresponds to the typical average dimension of the photospheric supergranular cells. This agreement of the scale of coronal structures and supergranules suggests the possible existence of a coupling of the coronal density fluctuations observed at 1.7 $R_\odot$ and photospheric convective motions at supergranular scale.

3.2. Structure Functions

The analysis of the structure functions and the scaling behavior of the coronal density fluctuations, aimed to assess the persistency, or memory, of the coronal density variations, is performed for timescales τ covering the range from hours to days, where the power spectra exhibit a power-law scaling. For the observed H I Lyα line intensity time series $\xi(t)$, consisting of N elements, the time-delayed differences $x(\tau) = \xi(t+\tau) - \xi(t)$ are functions of the delay τ. The statistical moments, namely the structure functions, of order $p > 0$ are estimated using the formula

$$\langle |x(\tau)|^p \rangle = \frac{1}{N} \sum_{n=1}^{N} |x_n(\tau)|^p. \quad (1)$$

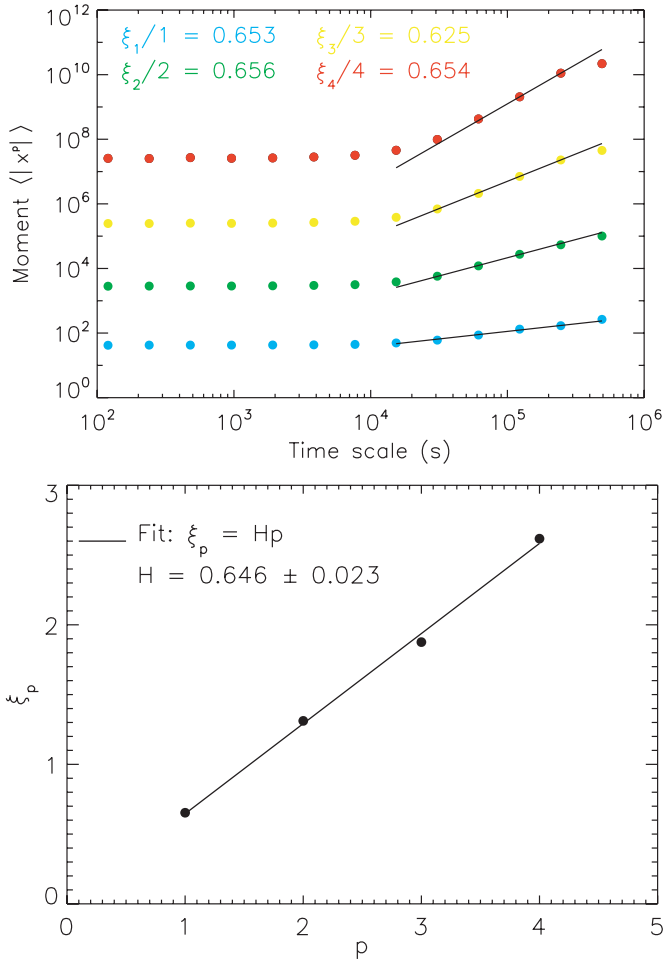

Figure 4. Top panel: the first four structure functions of the coronal density fluctuations at 7° NE as a function of timescale τ; the best linear fits are indicated as solid lines; the exponents ξ_p over the order p are shown for the four moments. Bottom panel: ξ_p exponent as a function of the order p of the moment: the linear fit leads to a constant Hurst exponent of $H = 0.646 \pm 0.023$.
(A color version of this figure is available in the online journal.)

The observed coronal density fluctuations exhibit a statistical self-similar scaling when the moment of order p scales as τ^{Hp}, satisfying the scaling power-law relation

$$\langle |x(\tau)|^p \rangle \propto \tau^{Hp}, \quad (2)$$

where the constant $H > 0$ is the Hurst exponent. Since the maximum value of the order of the moment, p_m, which can be optimally determined with a finite number N of points of the data sample, is given by the empirical criterion $p_m \backsimeq \log N$, the record of $N = 8192$ data points analyzed in this paper allows a reliable determination of the first four moments.

The structure functions calculated by using UVCS data in the equatorial region, at 7° NE, are shown in the top panel of Figure 4. Linear least squares fits on a log–log plot yield the power-law behavior $\langle |x(\tau)|^p \rangle \propto \tau^{\xi_p}$, with the exponents ξ_p shown in Figure 4. The fits show that the scaling exponent, ξ_p, increases linearly with the order of the moment, p, satisfying the relation $\xi_p = Hp$, as shown in the bottom panel of Figure 4. Hence, the scaling behavior is characterized by a single exponent H, leading to the conclusion that the coronal density fluctuations in the equatorial region exhibit a self-similar scaling for timescales τ larger than 10^4 s.

Table 2
Hurst Exponent H as a Function of Heliographic Latitude

Latitude (°)	Hurst Exponent, H
7 N	0.646 ± 0.023
1 S	0.686 ± 0.022
10 S	0.652 ± 0.019
18 S	0.673 ± 0.026
26 S	0.655 ± 0.023
34 S	0.602 ± 0.027
43 S	0.693 ± 0.022
51 S	0.600 ± 0.025

The analysis of the scaling of the structure functions is performed at each observed latitude, from 7° NE to 51° SE, although the accuracy decreases with the heliographic latitude. This is because at latitudes higher than 34° SE the coronal density fluctuations are observed at larger timescales (see Figure 3 and the cutoff frequency in Table 1); hence the best fit to the structure functions can be performed only over a few points, resulting in a less accurate estimate of the Hurst exponent. Nevertheless, at each latitude the coronal density fluctuations exhibit a self-affine scaling. The inferred Hurst exponent is reported in Table 2 as a function of heliographic latitude.

The Hurst exponent describes the persistency in a time series by testing the mutual dependence of the fluctuations in the time record and by searching for correlations between events. Since, for time series whose underlying processes are statistically independent, the random fluctuations are uncorrelated with a Hurst exponent $H = 1/2$, larger values of H indicate some persistency or memory in the time series. That is, in this case the signal is caused by a correlated stochastic process characterized by persistency. For the coronal data obtained in the latitude range considered in the analysis, the Hurst exponent is always larger than 1/2, with an average value $\langle H \rangle = 0.654 \pm 0.008$. This implies that the large-scale coronal density fluctuations are persistent at least up to 50° in latitude. Namely, the process underlying the variability of the midlatitude, equatorial solar corona and the slow coronal wind leads to a positive temporal correlation in the hydrogen Lyα intensity and, in turn, in the coronal plasma density time series.

Although the Fourier and the Hurst analyses are independent modes of investigation, the results obtained with these two techniques are related by the formula $\alpha = 2H + 1$. The average value of the Hurst exponent $\langle H \rangle = 0.654 \pm 0.008$ implies a spectral index $\alpha = 2\langle H \rangle + 1 = 2.31 \pm 0.11$, which is in good agreement with the one inferred from the Fourier analysis, $\langle \alpha \rangle = 2.36 \pm 0.07$ (see Table 1). In the hypothesis of stochastic, uncorrelated fluctuations, the power spectrum should exhibit a f^{-2} power law. Hence a spectral index α larger than 2 ($\alpha > 2$ implies $H > 1/2$) reveals a significant degree of persistency and correlation in the temporal series.

The degree of persistency observed in the coronal density fluctuations is consistent with the results of the Hurst analysis of photospheric intensity data obtained by Nesis et al. (1994). This fact suggests once more that the processes underlying the photospheric dynamics and coronal variability have common characteristics. Hence, this is considered a further indication of a likely connection of the density fluctuations observed in the outer corona and the intensity variations in the photosphere induced by the convective motions.

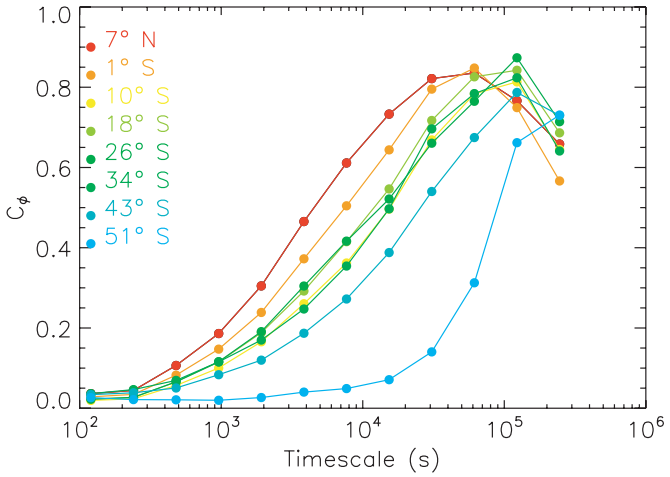

Figure 5. Phase coherence indexes c_ϕ of the coronal density fluctuations as a function of the timescale τ in the observed latitude coronal region.
(A color version of this figure is available in the online journal.)

3.3. Phase Coherence Index

The last step of the analysis is the investigation on phase coherence of the density fluctuations found in the outer corona. The phase coherence index (Hada et al. 2003),

$$c_\phi = \frac{L_{\rm PRS} - L_{\rm OBS}}{L_{\rm PRS} - L_{\rm PCS}}, \quad (3)$$

measures the degree of phase synchronization in a given observed time series (OBS), by comparing its first-order structure function $L = \langle |x(\tau)| \rangle$ with those of two surrogate time series derived from the observed data sample: (1) a phase-randomized surrogate data set (PRS), in which the phase of the Fourier basis functions are randomized, and (2) a phase-correlated surrogate data set (PCS), in which the values of the phases are all equal. In this procedure the amplitudes of the basis functions are kept the same as those of the observed time series. Thus the three data sets have the same Fourier power spectrum, but different phase distributions. At a given timescale τ, if the original data set is random in phase: $c_\phi(\tau) \approx 0$, while if the data set is completely phase correlated: $c_\phi(\tau) \approx 1$. This method is based on the fact that, when the phases are correlated, the time series appear to be smoother and the first-order moment smaller than in the case of random phases.

Figure 5 shows that the phase coherence in the coronal plasma density fluctuations does exist for timescales larger than about 10^4 s, in the full range of heliographic latitudes analyzed, although a higher degree of phase synchronization is reached at lower heliographic latitudes. This indicates that the coherent structures are mainly found in the static low-latitude streamers, rather than in the regions where the solar wind is accelerated.

The results shown in Figure 5 clearly indicate that the H I Lyα line intensity time series are dominated by structures coherent in phase. The origin of these coronal density structures is an open issue. Coherent structures could either arise from nonlinear interactions occurring in the corona itself or find their origin in the photosphere, those dynamics may act as a driver of the temporal variability observed in the outer solar atmosphere. This last hypothesis is suggested both by the Hurst analysis that has shown a similar degree of persistency of coronal and photospheric fluctuations and by the Fourier analysis that shows that the spatial scale of the coronal structures and supergranular cells are of the same order.

4. DISCUSSION AND CONCLUSIONS

Low and midlatitude observations of the outer solar corona emitting the H I Lyα line, obtained during solar minimum with UVCS at 1.7 $R_\odot$, provide new insights in the properties of the variability and the structure of the plasma density in coronal streamers and in the regions where the slow solar wind is accelerated. The power spectrum of the temporal evolution of the coronal plasma density, characterized by a power-law $f^{-\alpha}$ behavior with a spectral index $\alpha = 2.36 \pm 0.07$, is an evidence for the existence of large-scale coronal fluctuations in the latitude range from 7° NE to 51° SE, with periods from a few hours to a few days. This observational result can be interpreted as a signature of discontinuities in the time series, which separate spatial structures with a characteristic temporal scale of about 3 hr and a characteristic spatial scale of about 3×10^4 km, if such structures are corotating with the Sun.

The large-scale density fluctuations observed in the outer corona are statistically self-affine, namely they exhibit a fractal nature. That is, each part of the observed time series can be considered a reduced scale image of the whole. Furthermore, the nonlinear analysis based on the phase coherence index reveals that the coronal density is dominated by coherent structures. This feature is an evidence for either inhomogeneities locally generated by nonlinear interactions or nonpropagating instabilities carried by the expanding solar corona, at least in the regions where the slow solar wind is present.

The characteristics attributed to the coronal density fluctuations, such as the temporal and spatial scale, the degree of persistency and phase coherence, are all pointing to a likely association with the dynamics of solar convection and in particular to the supergranulation dynamics, although it is clear that the coupling of coronal variability and photospheric motions cannot be fully proved only on the basis of the observational evidence presented in this study.

The spatial scale of the coronal density structures, 3×10^4 km, is indeed consistent with the typical dimensions observed for photospheric supergranules, which show an average intercell spacing of about 3.2×10^4 km. The minimum temporal scale of the fluctuations in corona is 3 hr, thus including the lifetime of the photospheric supergranulation cells and the corresponding chromospheric network, higher up in the atmosphere, which is of about 20 hr on the average.

The degree of persistency of the density variations observed in the outer corona is consistent with that inferred by Nesis et al. (1994), who investigated the dynamics of the solar granulation, by analyzing the photospheric intensity oscillations. This unexpected agreement is an additional indication that we can hypothesize a coupling of photospheric convection and coronal variability and deduce that the Sun produces persistent and correlated variations, observed in the physical parameters of the solar atmosphere from the convective zone to the extended corona.

The results of the present study vary slowly moving from the coronal regions of closed to open magnetic configuration, where we find the streamers and the slow wind, respectively. We suggest however that the observed coherent structures, although maintaining a coupling with the supergranular motions in the photosphere, might be different in the two cases. In streamers, these plasma density structures are likely to be ascribed to processes occurring in the solar corona driven by the photospheric motions or propagating magnetoacoustic waves. While in the open-field regions we can presume that these

coherent structures can also be carried outward by the solar wind.

At present the photosphere–corona dynamic coupling can be only suggested for the equatorial and midlatitude regions, that is for the closed-field coronal streamer and the slow solar wind regions characterized by open magnetic field regions. While there is little evidence that it can be also invoked for the polar corona where the fast wind is emerging. Recent polar hole coronal density observations (Bemporad et al. 2008) have indeed shown that in the source region of the fast solar wind the coronal fluctuations exhibit a low-frequency f^{-2} power spectrum. This behavior, in the light of the discussion of the Hurst analysis of Section 3.2, indicates that the coronal density structures are temporally uncorrelated and statistically independent. Hence the comparison of the spectral index in the two cases shows that the coronal density variability in the fast wind differs from that observed at lower latitudes, where a spectral index α larger than 2 clearly indicates a relevant degree of persistency and time correlation in the observed time series. Thus, we can conclude that the coronal density structures observed in the fast and slow solar wind are characterized by a different degree of persistency.

This work was supported by the Italian Space Agency (ASI) grant (I/035/05/0). Daniele Telloni is a Ph.D. student with a fellowship of the National Institute for Astrophysics (INAF). UVCS is a joint project of the National Aeronautics and Space Administration (NASA), the Italian Space Agency and the Swiss funding agencies.

REFERENCES

Abbo, L., Antonucci, E., Dodero, M. A., & Carlo, B. 2003, in AIP Conf. Proc. 679, Solar Wind Ten: Proceedings of the tenth International Solar Wind Conference, ed. M. Velli, R. Bruno, & F. Malara (Melville, NY: AIP), 238
Antonucci, E., et al. 2005, A&A, 435, 699
Antonucci, E., et al. 2006, ApJ, 643, 1239
Bemporad, A., et al. 2008, ApJ, 677, L137
Berton, R. P. H. 2004, Nonlinear Process. Geophys., 11, 659
Bruno, R., et al. 2001, Planet. Space Sci., 49, 1201
Burlaga, L. F., & Mish, W. H. 1987, J. Geophys. Res., 92, 1261
Coles, W. A., & Harmon, J. K. 1978, J. Geophys. Res., 83, 1413
Gabriel, A. H. 1971, Sol. Phys., 21, 392
Hada, T., et al. 2003, Space Sci. Rev., 107, 463
Hoyng, P. 1976, A&A, 47, 449
Hurst, H. E. 1951, Trans. Am. Soc. Civ. Eng., 116, 770
Kohl, J. L., et al. 1995, Sol. Phys., 162, 313
Komm, R. W. 1995, Sol. Phys., 156, 17
Lepreti, F., et al. 2000, Sol. Phys., 197, 149
Mandelbrot, B., & Wallis, J. 1969, Water Resour. Res., 5, 321
Matthaeus, W. H., & Goldstein, M. L. 1986, Phys. Rev. Lett., 57, 495
Matthaeus, W. H., et al. 2007, ApJ, 657, 121
McComas, D. J., et al. 2000, J. Geophys. Res., 105, 10419
Morgan, H., et al. 2004, ApJ, 605, 521
Nesis, A., Hammer, R., & Hanslmeier, A. 1994, in ASP Conf. Ser. 64, Cool Stars, Stellar Systems, and the Sun, Proc. of the 8th Cambridge Workshop, ed. J.-P. Caillault (San Francisco, CA: ASP), 655
Noci, G., & Gavryuseva, E. 2007, ApJ, 658, L63
Noci, G., et al. 1987, ApJ, 315, 706
Roberts, D. A., & Goldstein, M. L. 1987, J. Geophys. Res., 92, 10105
Ruzmaikin, A., et al. 1994, Sol. Phys., 149, 395
Sari, J. W., & Ness, N. F. 1969, Sol. Phys., 8, 155
Siscoe, G. L., et al. 1968, J. Geophys. Res., 73, 61
Wang, Y. H., & Sheeley, N. R. 1990, ApJ, 355, 726
Wang, Y. H., et al. 2000, J. Geophys. Res., 105, 25133